

Formation Mechanism and Properties of Electrochemically Etched Trenches in n-Type Silicon

V. Lehmann¹ and H. Föll

Siemens AG, Technology Center for Microelectronics, D-8000 Munich 83, Germany

ABSTRACT

Three-dimensional structures in silicon are increasingly coming into use for the fabrication of mechanical and electrical devices. The fabrication of deep trenches is one of the most important problems in VLSI (very large scale integration) technology. In this study the spontaneous trench formation in n-type silicon immersed in hydrofluoric acid under anodic bias is demonstrated and the resulting microstructures are characterized. Trenches with arbitrary cross sections and high aspect ratios for microelectronic (e.g., 42 μm depth and 0.6 μm diam) and for power component application (e.g., 60 μm depth and 10 μm diam) have been produced by a standard masking technique. The trench formation is explained by a model which takes into account the conditions of the space charge region the minority carrier current and the crystal orientation. A passivating sidewall layer is not needed in this model. The dimensions and the shape of anodically etched trenches can be varied over a wide range by adjusting the critical parameters.

Since trench etching is becoming more and more important in silicon device fabrication, a large number of studies have been carried out to improve plasma etching techniques. However, submicron trench processes still suffer from structural effects which dominate the trench geometries [e.g., bottle-shaped profiles for trench opening which are smaller than a micrometer (1)]. Photoelectrochemically etched structures might be free of these shortcomings. They are, however, limited by the wavelengths of the penetrating light (2) so that submicron dimensions cannot be realized in that manner. In this work, an electrochemical etching technique will be presented which is independent of these geometrical restrictions.

The rate-determining step for an electrochemical dissolution process of silicon is either given by the number of holes (h^+) available at the electrode surface or by the diffusion-controlled flow of active ions to the electrode. In the latter case, the etch rate inside a trench must be smaller than the etch rate of the flat surface. As a consequence, the surface will be flat after some time. This effect is utilized for smoothing out surfaces and contributes to electropolishing (3). For the first case the reverse is true: if only few holes (h^+) are available at the electrode surface, the trench tips are more effective in collecting them from surrounding bulk material provided a space-charge region (scr) exists. Since anodic biasing of n-type silicon always creates a space-charge region, trench formation occurs spontaneously even at polished surfaces (4-6). The first section of this work reports about this phenomenon. In the second section the control of trench formation by masking is demonstrated and its viability for technology applications is shown. The parameters which determine trench growth are given in the third section. In the fourth section a model for the mechanism of electrochemical trench etching (ETE) is presented.

Experimental

The starting material consisted of n-type, (100) silicon wafers of various resistivities as listed in Table I. To evaluate the orientation dependence an additional (111) silicon sample (n-type, 1 Ωcm) was used. Samples of type A were as-received silicon wafers with a polished surface. Samples of type B and C had patterned layers (B samples: 20 nm SiO_2 , 150 nm Si_3N_4 , 1000 nm SiO_2 ; C samples: 900 nm SiO_2). The patterns were produced by a standard photolithographic process. The B samples had a pattern of circular 1 μm holes spaced at a distance of about 4 μm , i.e., approximately 15,000 holes per mm^2 (i.e., mask covering 98.8% of the surface, cf Fig. 5). The pattern in the C samples consisted of circular 10 μm holes spaced at a distance of about 30 μm , i.e., approximately 1000 holes per mm^2 (i.e., mask covering 92.5% of surface). Generally, every alkaline-resistant mask is suitable for ETE, because

the mask is only used for pre-etching the samples in KOH (cf. Masking procedure for electrochemical trench etching).

The size of the samples was 20 \times 20 mm (A samples) or 10 \times 10 mm (samples B and C) with a circular shaped area of 100 mm^2 (A sample) or 20 mm^2 (samples B and C) exposed to the electrolyte. An ohmic contact was provided by rubbing Ga-In eutectic around the circular area exposed to the electrolyte.

The samples was mounted in an electrochemical cell and connected to a potentiostat (Wenking POS 73). An additional ampere meter was used to measure the etching currents (Fig. 1). The applied voltage was measured in relation to a platinum wire positioned close (1 mm) to the sample surface. Considering the electrolyte concentration and the H_2 flow around the platinum wire (from the sample surface), the measured potential is presumably close to that of an NHE (normal hydrogen electrode) (7).

The electrolyte was 2.5 weight percent (w/o) (= 1.25 M/kg) hydrofluoric acid with a few drops per liter of a wetting agent ("Mirasol," registered trademark of Tetanal, Germany). It was stirred slightly during the experiments to remove hydrogen bubbles from the sample surface. All experiments were executed at room temperature.

During the electrochemical etching process, the samples were illuminated by a radiation from a 100W tungsten lamp. The window material used in the cell was Plexiglas, which is stable in hydrofluoric acid up to about 10 w/o. For some experiments, additional filters were used (a KG 5 filter which absorbs at wavelengths >800 nm or a GaAs filter which absorbs all wavelengths <867 nm).

The photocurrent, which is a parameter of interest for ETE, at n-type silicon is a nonlinear function of the illumination density (8). For back side illumination the diffusion

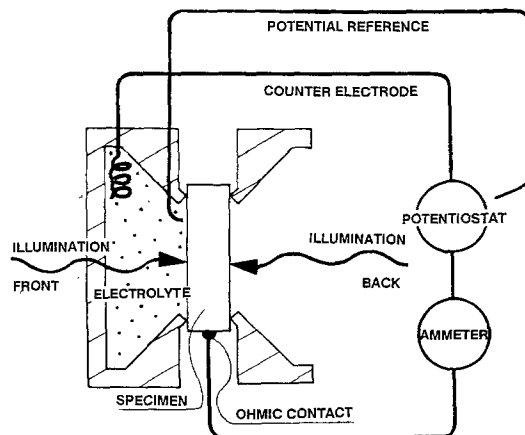


Fig. 1. Cross-sectional view of the electrochemical cell and its electrical connections.

¹ Present address: Department of Mechanical Engineering and Materials Science, Duke University, Durham, North Carolina 27706.

Table I. Resistivities of the used n-type silicon samples. A samples: polished surfaces. Samples B and C: masked surfaces

Sample	Ωcm	Sample	Ωcm	Sample	Ωcm
A1	0.01	B1	0.4	C1	60
A2	0.4	B2	1	C2	80
A3	0.8	B3	20	C3	200
A4	4				
A5	10				
A6	20				

length and the surface recombination velocity of the sample strongly influence the correlation between illumination and photocurrent (8). For that reason, the photocurrent was measured and not the illumination density. To give a reference point, a p-type silicon sample in the described setup (Fig. 1) under reverse bias, illuminated with 100 mW/cm^2 , will produce a photocurrent of 30 mA/cm^2 .

Concurrent with the common usage and to avoid ambiguity, all etched structures in the following will be called trenches. The expression hole will only be used for defect electrons (h^+).

Results and Discussion

Anodic dissolution of illuminated n-type silicon.—A silicon electrode is dissolved in an acidic electrolyte which contains F^- ions if holes (h^+) are available. For a p-doped sample under anodic bias, this condition is always fulfilled. The anodic region of the current density vs. voltage curve for p-type silicon is shown in Fig. 2.

Electropolishing occurs for current densities exceeding a critical current density J_{PSL} . For current densities below J_{PSL} , the dissolution process is changing and a porous silicon layer (PSL) grows on the silicon surface (9-14).

In n-type silicon, holes (h^+) can be generated by illumination or by high electrical field-strength. For high illumination densities, the current-voltage curve of n-type silicon was found to be identical to that of p-type silicon with the exception of a few hundred mV shift on the voltage axis. By adjusting the illumination, all points beneath the p-type anodic current-voltage curve (shaded region in Fig. 2) can be reached. Trench formation has only been observed for n-type silicon and current densities below J_{PSL} .

Trench formation in n-type silicon anodically biased in the dark has been described by Theunissen *et al.* (4, 5). The resulting channels are needle-shaped and strongly branched.

If the sample is illuminated during anodization, this geometry changes. Sample A2 was anodized for 30, 60, 120, and 240s at 14V bias. The lamp was operated at 30W electrical power to enhance the infrared contribution of the spectrum (no additional filters, front side illumination). The photocurrent was adjusted to 10 mA/cm^2 by varying the

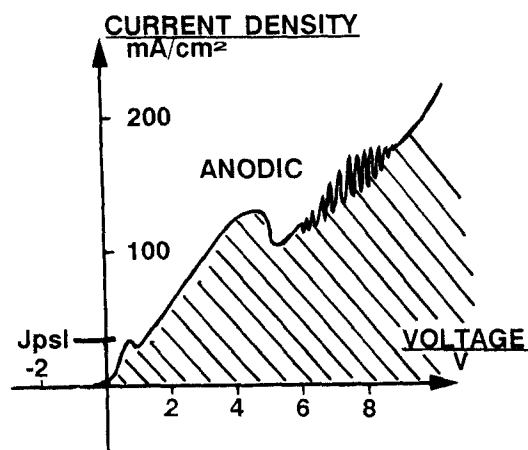


Fig. 2. Anodic region of the current-voltage curve for p-type (and strongly illuminated n-type) silicon in contact with an electrolyte of hydrofluoric acid. For n-type silicon all points in the shaded region can be reached by adjusting the light intensity; trench growth was observed for current densities below J_{PSL} .

distance to the lamp. J_{PSL} is a function of the HF concentration and the stirring conditions. For 2.5 w/o HF, the critical current density J_{PSL} is about 20 mA/cm^2 . Scanning electron microscope (SEM) micrographs of these samples are shown in Fig. 3a-d. The etched trenches are covered with a layer of porous silicon (PSL) of about 100 nm. To reveal the geometry of the resulting channels more clearly, the PSL is easily removed by immersion in 10 w/o aqueous solution of KOH for 10s at room temperature followed by rinsing in deionized water (5 min). This procedure has been performed in all following examples.

Figures 3e-h show SEM micrographs of the samples without PSL at a viewing angle of 40° . The surface (90°) is shown in Fig. 3i-m. This microscopic honeycomb-like surface absorbs light to an extremely high degree *i.e.*, macroscopically and has a pitch-black appearance. The reflectance index (240s sample) was determined to be <0.0001 for 0° reflective angle and <0.0005 for 90° by laser reflection measurements (633 nm HeNe).

To investigate the wavelength-dependence of the trench formation, the samples were illuminated by radiation of different wavelengths by using filters. All other parameters were kept constant (photocurrent: 10 mA/cm^2 , voltage: 14V). No trench formation was observed for a KG 5 filter which absorbs at wavelengths $>800 \text{ nm}$. Using a GaAs filter which absorbs at wavelengths $<867 \text{ nm}$, the vertical cross section of the trenches changed from a conical to a cylindrical shape.

These results can be understood if the local minority carrier generation rate determines the trench shape in the following manner: carriers which are generated deep in the bulk promote the trench growth at the tips, whereas near-surface generation leads to lateral growth of the trenches. To prove this hypothesis, an A2 sample was illuminated from the back side of the wafer. In this arrangement, the

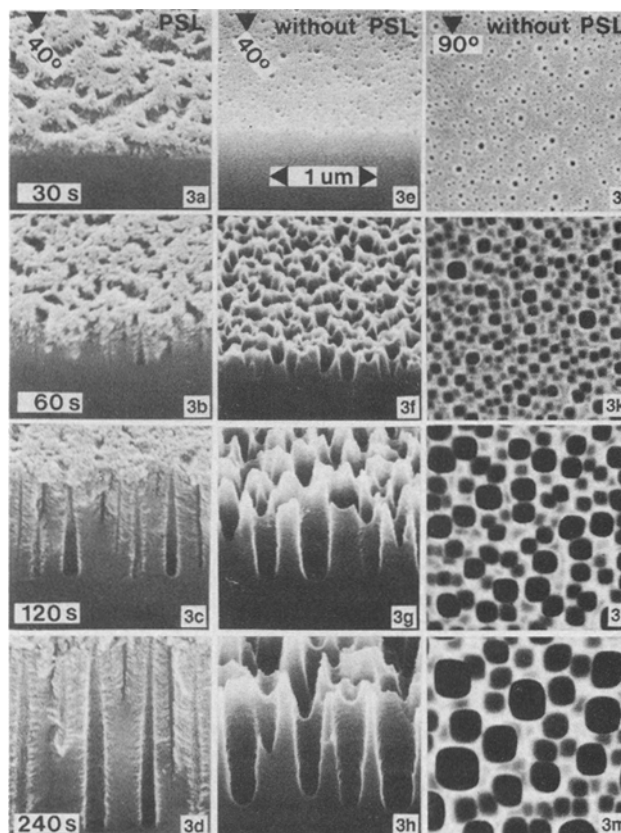


Fig. 3 (a-d) SEM micrographs (cross section, 40°) of electrochemically etched n-type samples (A2). The shown (front) side of the samples was illuminated during anodization (+14V, 10 mA/cm^2) for the indicated times. The trenches are covered with porous silicon (PSL). (e-h) SEM micrographs (cross section, 40°) of the samples after immersing the samples in 10 w/o KOH for 10s to remove the covering porous silicon layer (PSL). (i-m) SEM micrographs (plan view, 90°) of the samples (PSL removed).

minority carriers had to diffuse through the sample to reach the trench tips [for more information about the diffusion process, see (8)]. In this experiment and all following with back side illumination, a KG 5 filter was used. The trenches produced in this manner were cylindrical and orthogonal to the (100) surface. Their length was a linear function of the anodization time and the surface was not corroded, with the exception of the trench openings. From these results it is concluded that the region between the trenches is almost depleted and practically all carriers coming from the bulk region are collected by trench tips. This is illustrated in Fig. 4a which shows the schematic distribution of the electric field lines which leads to that collecting mechanism.

Both methods, front side and back side illumination, lead to a wide scatter in diameters of the etched trenches. The diameter depends on the local efficiency in capturing minority carriers, which is determined by the initial position of the trench in the random trench pattern. Figures 3i-m illustrate this. After 30s anodization time, more than 100 small trenches per μm^2 were generated (Fig. 3i), but only 5-10 per μm^2 survived after 240s (Fig. 3m). The density of trenches is a function of doping density and pitting conditions, but it was found to be $>10^6/\text{cm}^2$ in all cases for (100) surfaces.

To evaluate the orientation dependence of ETE, a (111) sample (n-type, $1 \Omega\text{cm}$) was etched in 2.5 w/o HF for 65 min at $500 \mu\text{A}/\text{cm}^2$ (back side illumination) and analyzed by SEM. Figure 4b shows the difference in geometry of trenches grown in (100) and (111) material. It is evident that the trench tips in both cases are growing in the $\langle 100 \rangle$ direction.

As expected for current densities below J_{PSL} , hydrogen evolution was observed at the sample surface during anodization (3).

Masking procedure for electrochemical trench etching.—To make this method a useful tool in device fabrication, it is essential to be able to position trenches in distinct patterns. If a random pattern of etch pits (cf. Fig. 3i) generates a random trench pattern, a regular pattern of pits should produce regularly spaced trenches. To produce the necessary pit pattern, masked n-type samples (B + C) were pre-etched in KOH (10 w/o aqueous solution), which generates the well-known anisotropic etch figures (15). In (100) silicon a pyramidal-shaped hole is formed (Fig. 5) which was found to be sufficient to induce ETE.

Using these pre-etched samples, the trench geometry was studied for different doping densities, photocurrents, voltages, and etching times. The oxide mask is rapidly dissolved by immersing the samples in the electrolyte which contains hydrofluoric acid so that the whole surface is exposed to the electrolyte. It should be noted that after formation of the pyramidal shaped-depressions, no subsequent mask of any type is necessary for trench growth.

Figures 6a-c show the vertical cross sections of the trenches (drawings for SEM micrographs) as a function of the applied voltage and photocurrent (back side illumination). The etching time of all samples was 30 min. At 10V bias the anodic current for sample B1, which had the highest doping density, exceeds 1 nA/trench even without any illumination (Fig. 6a). For the B2 samples (Fig. 6b) it was impossible to reduce the current to 33 pA/trench at 10V bias. Electrical breakdown at the trench tips was assumed to be the reason for these high dark currents. This mechanism will be discussed later.

Figure 6d illustrates the degeneration of the circular (horizontal) cross section of the trenches for higher voltages. This phenomenon will be termed "branching" in the following and occurs along the whole vertical length of the trench. A point worth noting is that the branches are growing in the $\langle 100 \rangle$ direction.

For samples with a high doping density (B1), it was found that there is a tendency for a trench to divide in two or four separate trenches. For low-doped samples (B3), the reverse is true; the number of trenches decreases, while the diameter of the surviving trenches increases by the higher current-per-trench ratio. This is schematically shown in Fig. 6e.

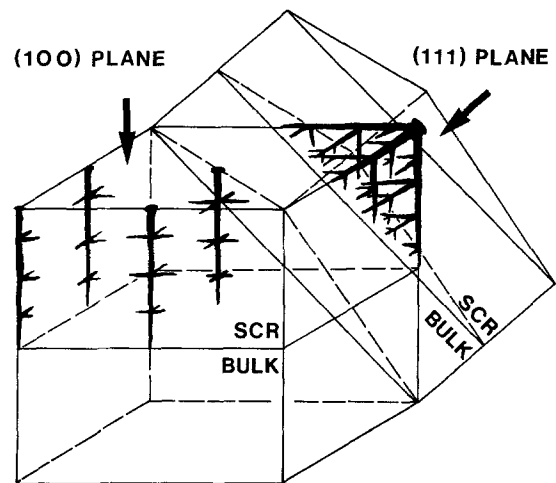
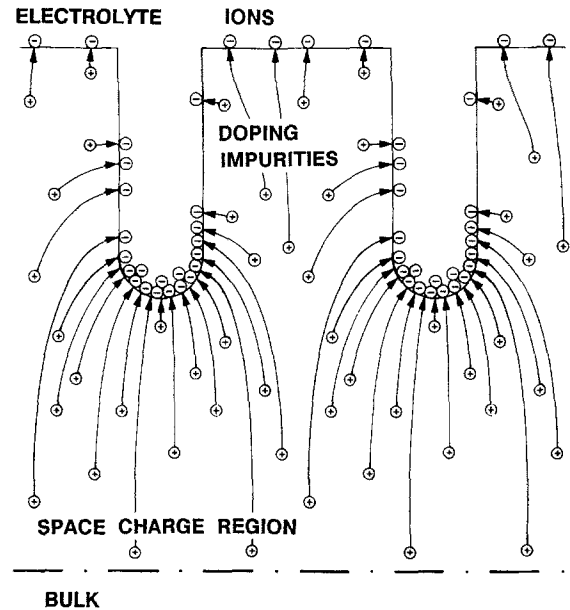


Fig. 4. (a, top) Schematic distribution of the electric field lines in the space charge region around the trenches during anodization in the electrolyte. (b, bottom) Trench configuration as a function of the crystal orientation of the silicon sample. (Drawings from SEM micrographs.)

Excluding the cases of no significant trench growth, all trenches shown in Fig. 6a, b, and c have about the same depth, even if parameters like doping, voltage, or current differ one order of magnitude. In 45 experiments with different conditions of masking, doping, voltage, and current, the growth rates of trenches were measured (Fig. 7). The growth rates average around $0.5 \mu\text{m}/\text{min}$. For a constant set of parameters, the depth was found to be a linear function of time.

To determine the number of charge carriers, n , which was necessary to dissolve one silicon atom, a C2 sample was anodized at 1V, 13.3 nA/trench for 100 min (Fig. 11). The diameter of the resulting trenches is approximately $10 \mu\text{m}$ producing a sectional area of $78.5 \mu\text{m}^2$ and a current density $J = 16.94 \text{ mA}/\text{cm}^2$. This current density and the etch rate of $0.6 \mu\text{m}/\text{min}$ (trench depth $D = 60 \mu\text{m}$ in $t = 100 \text{ min}$) produce a dissolution valence of $n = 2.12$ using

$$n = tm_{\text{Si}}J/(ed_{\text{Si}}V_{\text{D}})$$

V_{D} = dissolved volume, e = elementary charge, m_{Si} = mass of a Si atom, d_{Si} = density of Si. This result is in good agreement with the known dissolution valence of silicon for currents below J_{PSL} which is $n = 2$ (3, 9).

To evaluate if there is a maximum depth for electrochemically etched trenches, a C2 sample was anodized at 1V, 13.3 nA/trench for 12h. This would produce trenches of

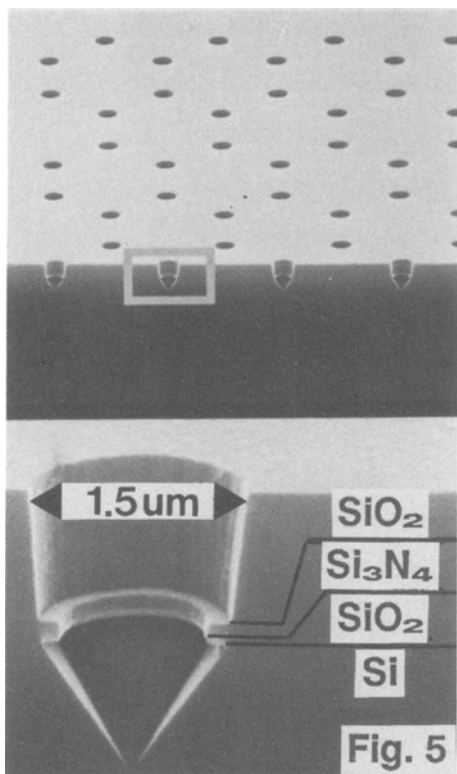


Fig. 5. SEM micrograph (cross section, 40°) of an n-type sample (B1) which was masked and pre-etched in KOH.

a depth exceeding 400 μm if the etch rate is a constant 0.6 $\mu\text{m}/\text{min}$. But the cross section of these sample showed cylindrical trenches of 300 μm depth with cavities at their tips of about 30 μm diam. Possibly the electrolyte concentration decreased in the long trenches to a value that makes the critical current density J_{PSL} smaller than J , which produces electropolishing conditions at the bottom of the trenches. For higher HF concentrations, trench growth through the entire wafer thickness should be possible.

To test whether the growth of a pattern of trenches is uniform in depth for all trenches, a C2 sample was anodized at 1V, 13.3 nA/trench for 100 min (Fig. 11). This sample was mechanically thinned from the back side and the depth distribution of a field of $32 \times 32 = 1024$ trenches was analyzed. The depth D of nearly all trenches (1012) was within the range $59 < D < 63 \mu\text{m}$, nine trenches are in the

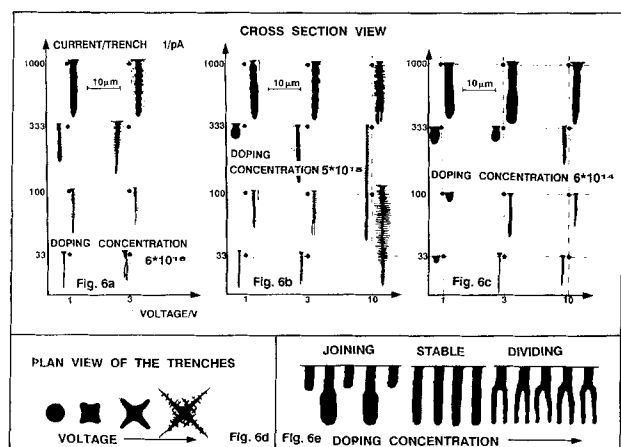


Fig. 6. (a-c) The trench shape as a function of doping (cm^{-3}), current per trench, and voltage of anodization. (Samples: B1, B2, and B3; drawings of sample cross section, 0°, from SEM micrographs.) (d) Degeneration of the circular trench cross section for higher anodic bias. (Drawings from SEM micrographs, plan view 90°.) (e) Schematic dividing and joining of trenches.

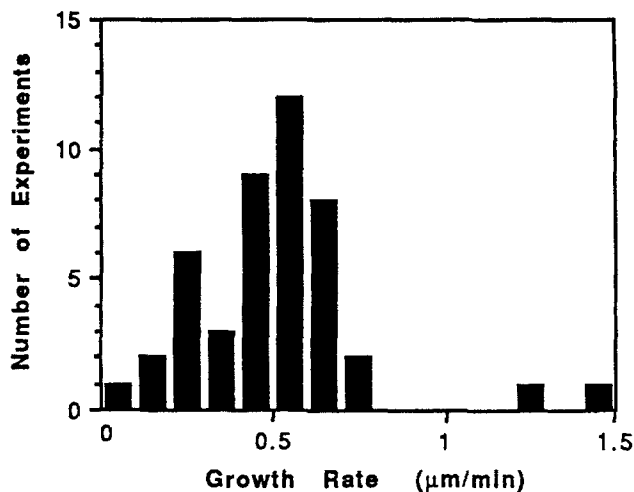


Fig. 7. Observed growth rates of electrochemically etched trenches for experiments with different values of voltage, current, and doping. (All parameters were held constant during the etching time of a single experiment.)

depth range $49 < D < 59 \mu\text{m}$ and only three trenches of a lower depth were found.

In no case was trench growth found in masked or unmasked p-type silicon samples.

Parameters influencing electrochemical trench etching.—The results presented in the foregoing section show that the pattern of trenches and their shape is controllable by an appropriate masking procedure. The different parameters which determine the geometry of the trenches interact, but to make the results surveyable we attempt to relate them to properties of the etched trenches.

Anodization time.—The trench depth D is a linear function of the anodization time t : $D = ct$, the constant c is a weak function of the other parameters. This means even for differences of one order of magnitude in voltage, current, or doping density, the etch rates were found to average around 0.5 $\mu\text{m}/\text{min}$ (Fig. 7).

Photocurrent.—The current density J at the etched surface has to be lower than the critical current density J_{PSL} to produce ETE. The product of photocurrent and time determines the volume dissolved. Since the etching time determines the trench depth, the hole diameter is proportional to the square root of the photocurrent. If the current density is varied during the etching process, the diameter of the trenches will vary accordingly. Branching is reduced for higher current densities.

Applied voltage.—For low voltages ($< 1\text{V}$ with respect to the Pt electrode) no trench formation occurs. For higher voltages trenches will grow if minority carriers are available in the bulk, e.g., generated by illumination. Above a doping dependent critical voltage, needle-shaped trenches will grow even if the sample is not illuminated. Electrical breakdown is supposed to be the reason for this (5). With increasing voltage the horizontal cross section of the trenches degenerate from a round to a dendritic shape (cf. Fig. 6d).

Starting surface conditions (masking).—As shown above, a polished surface results in a random arrangement of trenches ($> 10^6/\text{cm}^2$). The collecting area for minority carriers and consequently the diameter for each trench is determined by the distance to the neighboring trenches. With masking techniques the pattern of trenches is controllable within the limits given by the doping density. For example, if the trench density given by the masking is too high in relation to the doping density, the trenches join. In the reverse case dividing occurs (cf. Fig. 6e). It is important to note that the typical concept of a mask, covering all surfaces between desired pits, is not necessary. A simple pattern of depressions in the surface is enough to initiate ETE.

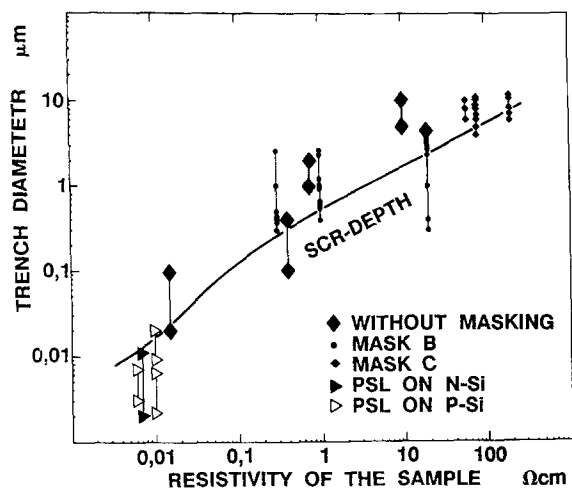


Fig. 8. Depth of the space charge region (for 1V bias) and diameter of PSL pores (10-12) and electrochemically etched trenches as a function of sample resistivity.

Doping density.—The n-type doping density determines the range of stable hole diameters. If current density and masking would lead to diameters larger or smaller than the range of stable diameters, the trenches begin to divide or join (cf. Fig. 6e). In Fig. 8 the observed trench diameters are shown as a function of the doping density. The diameters of the trenches are in reasonable agreement with the doping dependent width of the space charge region. Branching increases with increasing doping density.

Place of minority carrier generation.—Front side illumination with short wavelength (<800 nm) produces a homogeneously etched surface. The unfiltered lamp radiation gives cone-shaped trenches. Their depth is limited by this geometry and depends on the wavelength distribution. Back side illumination produces cylindrical trenches. Of course, nonuniformities of the illumination or the minority carrier lifetime will lead to nonuniform current densities (8) and consequently to different trench diameters.

Crystal orientation.—According to Fig. 4a, the direction of the trench growth should be orthogonal to the boundary plane between space charge region and bulk. Figure 9 demonstrates that this is indeed the case for (100) samples. The trenches grow in the <100> direction with high precision. For (111) silicon the trench tips are still growing preferably in the <100> direction. For (111) material the (100) planes are not orthogonal to the surface and the trenches develop a fir-tree shape by continuous dividing. In both cases, however, the boundary-plane between the space charge region and bulk material determines the overall direction of trench growth; Fig. 4b illustrates this.

The trench geometry is controllable within the limits imposed by these parameters. This is illustrated by SEM micrographs (Fig. 9-11) which show a great variety of trench dimensions and aspect ratios.

Model for the formation mechanism of electrochemically etched trenches.—The dissolution of nonilluminated n-type silicon under anodic bias in HF is discussed in detail by Theunissen *et al.* (4, 5). In short, if the electrical field exceeds a critical breakdown field strength (16), spontaneous trench growth occurs even at polished surfaces. The electrical field strength increases with increasing doping density and applied voltage. If trenches have developed, the breakdown field strength is reached even for lower voltages by the geometrical field enhancement around the trench tips (cf. Fig. 4a), which leads to point discharge. This effect is the reason, by the way, for nonreproducible current-voltage curves for the anodic region of n-type silicon. Trenches generated by breakdown will be needle shaped and strongly branched. The chemical reaction is

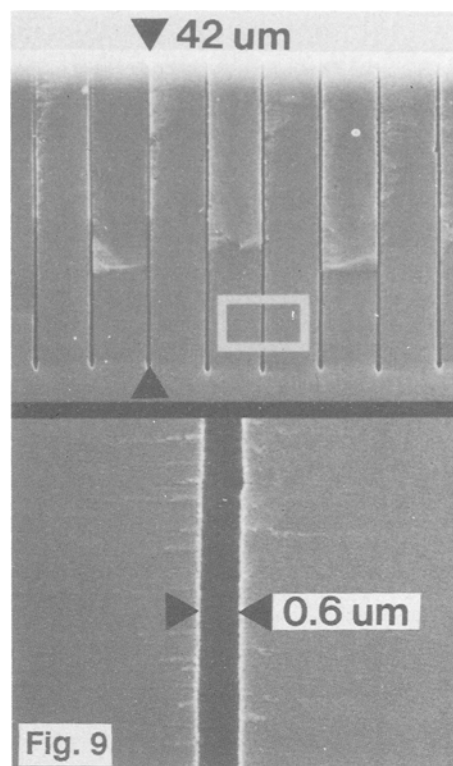
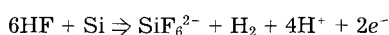


Fig. 9. SEM micrograph (cross section, 0°) of electrochemically etched trenches with high aspect ratio. (B2 sample, 10V, 30 min, 330 pA/trench; all three samples: photocurrent adjusted by back side illumination, PSL removed by 10s in 10 w/o KOH.)

The electrons are injected into the bulk by point discharge at the trench tips.

If the sample is illuminated while etching, the photocurrent becomes an additional parameter (besides the breakdown current). If the breakdown mechanism is sup-

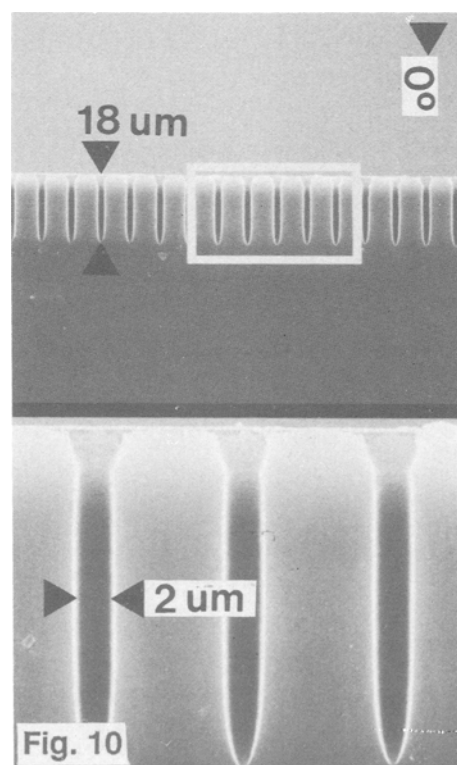


Fig. 10. Micrograph of trenches with larger diameter produced with the same mask as trenches in Fig. 9. (B3 sample, 10V, 30 min, 1 nA/trench.)

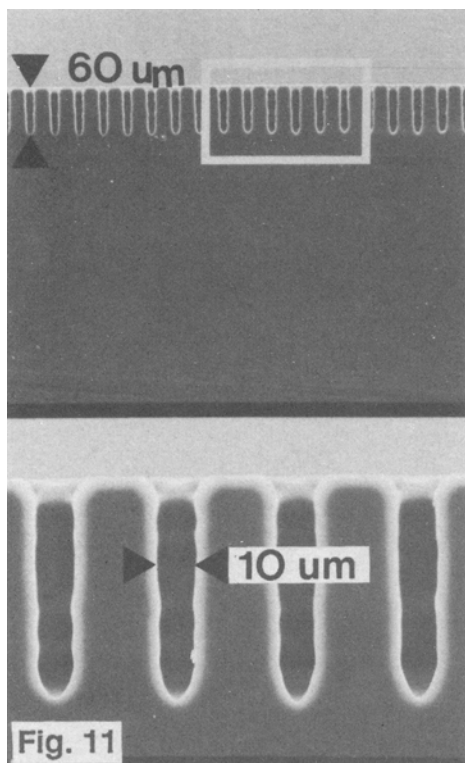
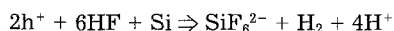


Fig. 11. Trenches with large dimensions produced with mask C. (C2 sample, 1V 100 min, 13.3 nA/trench.)

pressed (for low voltage, low doping, high photocurrent), the growth of every trench is determined by its success in collecting photogenerated minority carriers. If the trenches are spaced in equal distances (by masking) they will have equal growth rates. In this case (no breakdown) the trench walls will be smooth and no branching occurs.

If samples are anodized without masking, the diameter of the resulting trenches will be doping dependent and therefore in agreement with the width of space charge region in this material. If there is a significant misfit between this stable diameter and the trench spacing the trenches will join or divide. The reaction scheme is identical with the reaction mentioned above with the exception that photogenerated holes ($2h^+$) are necessary to induce the reaction at the trench tips



If one assumes that a layer exists which protects the walls from being etched, the observed doping dependence of the effect would be inexplicable. From these results it is concluded that the space-charge region itself protects the trench walls from being etched. The borderline between space-charge region and bulk is a plane beneath the trench tips. In other words, the whole region between the trenches is depleted. If all minority carriers are collected by the trench tips there are none left to permit etching of the wall. This means that a depletion effect is the reason for ETE, not an inhibition layer of a different chemical composition at the trench walls.

From these findings, the charge transfer at the tips and not mass transfer in the trench is proposed to be the limiting step for trench growth. If this is true, the fast mass transfer in the small trenches and the even faster one in the narrow PSL pores are still open questions.

The hydrogen evolution probably occurs at the trench openings, in other words there are no bubbles in the trench. This is concluded from observations of small ($<100 \mu\text{m}$) cathodic hydrogen bubbles during experiments investigating defects in SiO_2 layers (17). When the hydrogen generating cathodic current is switched off, bubbles which are smaller than $100 \mu\text{m}$ decrease in diameter and disappear after several seconds. This is understandable

due to the high-pressure P in small bubbles, defined by $P = P_0 + 2\sigma/r$ (radius r , surface tension σ , ambient pressure P_0).

The strong dependence of the trench growth on crystal orientation might be a result of slightly different etch rates for different crystal planes at the trench tips. This will produce a cone-shaped tip profile (Fig. 10 and 11) with the highest field strength at its center, adjusting the growth direction to $\langle 100 \rangle$.

This hypothesis may also give some new insight for PSL growth. The measured pore diameters of PSL (10-12) grown on degenerate silicon samples are in agreement with the trench diameter dependence on doping density shown in Fig. 8. In addition, TEM images of PSL in degenerate (100) silicon show pores orthogonal to the surface (10). The growth of PSL on degenerate silicon is assumed to be similar to ETE with smaller trenches depending on the higher doping density.

PSL in nondegenerate silicon is found to be different from PSL in degenerate silicon (10, 11, 13). The very low conductivity (14) and the transmittance for visible light (even for porous layers up to $50 \mu\text{m}$) indicate a difference between the band structure of bulk silicon and the resulting PSL. Nevertheless, it may be presumed that the PSL growth in nondegenerate silicon is also a depletion effect. Contrary to the depletion region generated by an applied voltage, the depletion occurs directly from the very narrow [$<2 \text{ nm}$ (11)] pores, which by themselves strongly disturb the periodic potential in the small material regions remaining between them.

Finally, we would like to mention the surprising similarity between the properties of ETE and the channels etched in aluminum foils. If an aluminum sample is anodized in halide containing electrolytes, a high density ($10^7/\text{cm}^2$) of etch channels is produced and the direction of growth is $\langle 100 \rangle$. The tunnel walls and the sample surface are apparently passive. The growth rate ($1-10 \mu\text{m}/\text{min}$) is a linear function of time and insensitive to the other parameters. The aluminum must be very pure for channel etching, even different lots of high purity (99.99%) show different properties (18, 19). By photocurrent measurements, a semiconducting intermediate phase of aluminum oxide was found with a smaller bandgap (2-3.5 eV) than Al_2O_3 (8-9 eV) (20).

The objection that there is no depletion between the channels in aluminum is justified. But for trench growth only an insoluble, insulating layer is assumed by the presented hypothesis which makes the tips more effective in collecting charge carriers by their higher electrical field strength. This layer may be insulating by a different chemical (aluminum oxide for Al) or electronic (the space charge region for Si) composition. It is not essential, whether the charge transfer occurs by breakdown, by tunneling of electrons, or by generation of charge carriers in a semiconductive layer (either by illumination or by high field strength). In any case, the electric field enhancement which originates in the geometry of the trench tip itself is assumed to be the driving force in the electrochemical trench etching mechanism in aluminum, just as in silicon.

Conclusions

Electrochemically grown random trench patterns on n-type silicon offer new possibilities for generating surfaces with high absorption coefficients. They might be useful as emitting sources (black bodies) or for collector applications (solar cells). The possibility of localizing electrochemically etched trenches in a feasible pattern by a masking procedure and their controllable shape permits a multitude of applications in electronic and micromechanic devices. Studying the pitting and trench growth effects in a well-understood material like silicon might give some new insights for corrosion mechanisms.

Manuscript submitted March 31, 1989; revised manuscript received ca. Sept. 1, 1989.

Siemens AG assisted in meeting the publication costs of this article.

REFERENCES

1. D. Chin, S. H. Dhong, and G. J. Long, *This Journal*, **132**, 1705 (1985).
2. M. M. Carrabba, N. M. Nguyen, and R. D. Rauh, *ibid.*, **134**, 1855 (1987).
3. D. R. Turner, *ibid.*, **105**, 402 (1958).
4. M. J. J. Theunissen, J. A. Appels, and W. H. C. G. Verkuylen, *ibid.*, **117**, 959 (1970).
5. M. J. J. Theunissen, *ibid.*, **119**, 351 (1972).
6. M. J. Hill, *ibid.*, **120**, 1425 (1973).
7. D. J. G. Ives and G. J. Janz, "Reference Electrodes, Theory and Practice," p. 71, Academic Press, New York, London (1961).
8. V. Lehmann and H. Föll, *This Journal*, **135**, 2831 (1988).
9. Y. Arita and Y. Sunohara, *ibid.*, **124**, 285 (1977).
10. M. I. J. Beale, N. G. Chew, M. J. Uren, A. G. Cullis, and J. D. Benjamin, *Appl. Phys. Lett.*, **46**, 86 (1985).
11. R. Herino, G. Bomchil, K. Barla, and C. Bertrand, *This Journal*, **134**, 1994 (1987).
12. F. Phillip, K. Urban, and M. Wilkens, *Ultramicroscopy*, **13**, 379 (1984).
13. C. Pickering, M. I. J. Beale, D. J. Robbins, P. J. Pearson, and R. Greef, *J. Phys. C: Solid State Phys.*, **17**, 6535 (1984).
14. T. Unagami, *This Journal*, **127**, 476 (1980).
15. K. E. Bean, *IEEE Trans. Electron Devices*, **ED-25**, 1185 (1978).
16. A. S. Grove, "Physics and Technology of Semiconductor Devices," p. 193, John Wiley and Sons, Inc., New York (1967).
17. H. Wendt, H. Cerva, V. Lehmann, and W. Pamler, *J. Appl. Phys.*, **65**, 2402 (1989).
18. K. Hebert and R. Alkire, *This Journal*, **135**, 2146 (1988).
19. K. Hebert and R. Alkire, *ibid.*, **135**, 2447 (1988).
20. S. Menezes, R. Haak, G. Hagen, and M. Kendig, *ibid.*, **136**, 1884 (1989).

A Mathematical Model for Silicide Oxidation

S.-L. Zhang

Fasta Tillståndets Elektronik, Kungliga Tekniska Högskolan-Electrum, 164 28 Kista, Sweden

R. Ghez*

IBM T. J. Watson Research Center, Yorktown Heights, New York 10598

F. M. d'Heurle

*Fasta Tillståndets Elektronik, Kungliga Tekniska Högskolan-Electrum, 164 28 Kista, Sweden
and*

IBM T. J. Watson Research Center, Yorktown Heights, New York 10598

ABSTRACT

Silicide layers on silicon can be thermally oxidized in such a way as to grow a layer of (metal-free) SiO_2 without affecting the integrity of the silicide. The conditions necessary for this to occur depend on the rate of silicon (or metal) transport through the silicide, and on the rate of oxygen consumption at the silicide/oxide interface. These conditions can be defined in terms of the thermodynamics of silicon and metal oxidations. One obtains two equations for transport through the respective layers and one for the chemical reaction rate at the silicide/oxide interface. The simultaneous solution of these three equations enables one to determine (at least theoretically): (i) the maximum allowable drop in silicon activity at that interface, and (ii) under what conditions the metal in the silicide would oxidize concurrently with silicon.

With some exceptions [see Ref. (1)], under the proper conditions (2-5), silicide layers on a silicon substrate can be thermally oxidized with the formation of pure SiO_2 , without any metal oxidation. How is this possible? The question has received various answers, some have emphasized (6) the kinetic aspects of the question, others (7-9) have rightfully shown that the phenomena are largely dominated by thermodynamic considerations. (In this respect one notes that during oxidation one has a system of three components—metal, silicon, and oxygen—and four phases—silicon, silicide, oxide and oxygen. At constant temperature and pressure such a system cannot be in a condition close to equilibrium; that would violate the phase rule.) Historically the problem may be seen as a special case of the more general problem of alloy oxidation, that was the object of two articles (10, 11) in this journal many years ago. Therein one may find the oxidation conditions under which a single oxide is formed over a binary alloy. Since this is largely a matter of the sufficiently rapid diffusion of atoms within the metal matrix being oxidized, there is a tendency to see the problem and its solution in kinetic terms. However, there exists in this case a very strong, yet subtle, correlation between kinetics and thermodynamics that has been revisited (12) a few years ago. For the special case of the silicides, this has been expressed (5) completely only by graphical means. The differential equations and their solution were presented (13)

earlier but with emphasis on kinetics per se, rather than the thermodynamic implications. The model here follows the pattern established for the derivation (14, 15) and interpretation (16, 17) of the linear-parabolic law of oxidation, that is well known to those familiar with silicon technology. The treatment will be almost purely mathematical; for an analysis of the physical problems of diffusion, decomposition, etc. which enter in studies of silicide oxidation, the reader should consult one of several available reviews, especially Ref. (2, 4, and 5). For thin silicide layers, and/or extremely fast diffusion in these layers, one finds the usual linear-parabolic equation, whose practical validity even for silicide oxidation was established (18, 19) previously. However, the solution remains nearly linear-parabolic even away from such limiting conditions.

For a multiplicity of reasons only the formation of pure SiO_2 will be considered. To begin with this is the only subject that has been investigated thoroughly, with perhaps only one exception, the oxidation of NbSi_2 on a SiO_2 substrate, resulting in the formation of a mixture (20) of oxides. With another silicide that is widely used in current electronic technology, WSi_2 , metal oxidation results in the formation of volatile tungsten oxides. These blister through the layer of SiO_2 and destroy its integrity. The formation of silicates is conceivable but of limited interest since it would damage the silicide layer. With TiSi_2 (to be mentioned again later), the oxide equilibrium diagram (21, 22) shows no intermediate phases between TiO_2 and SiO_2 and limited solubility of TiO_2 in SiO_2 . Some silicides

* Electrochemical Society Active Member.